*Environ. Sci. Technol.* **2010,** *44,* 7839–7845

# Interactions of Oxytetracycline with a Smectite Clay: A Spectroscopic Study with Molecular Simulations

LUDMILLA ARISTILDE,*,†,⊥ CLAIRE MARICHAL,‡ JOCELYNE MIÉHÉ-BRENDLÉ,‡ BRUNO LANSON,§ AND LAURENT CHARLET†,∥

*Environmental Geochemistry Group, LGIT, and Mineralogy and Environments Group, LGCA, University of Grenoble-1, CNRS, F-38041 Grenoble, France, Equipe Matériaux à Porosité Contrôlée, IS2M, CNRS 7228, Université de Haute Alsace, 68093 Mulhouse, France and Institut Universitaire de France, 75005 Paris, France*

*Received June 24, 2010. Revised manuscript received September 7, 2010. Accepted September 7, 2010.*

Binding of antibiotics to clay minerals can decrease both their physical and biological availability in soils. To elucidate the binding mechanisms of tetracycline antibiotics on smectite clays as a function of pH, we probed the interactions of oxytetracycline (OTC) with Na-montmorillonite (MONT) using X-ray diffraction (XRD), infrared (IR), and solid-state nuclear magnetic resonance (NMR) spectroscopies, and Monte Carlo molecular simulations. The XRD patterns demonstrate the presence of OTC in the MONT interlayer space at acidic pH whereas complexation of OTC by external basal and edge sites seems to prevail at pH 8. At both pH, the $^{1}H-^{13}C$ NMR profile indicates restricted mobility of the adsorbed OTC species; and, $-CH_3$ deformation and C—N stretching IR vibration bands confirm a binding mechanism involving the protonated dimethylamino group of OTC. Changes in the $^{23}Na$ NMR environments are consistent with cation-exchange and cation complexation reactions at the different sites of adsorption. Molecular simulations indicate that MONT interlayer spacing and structural charge localization dictate favorable binding conformations of the intercalated OTC, facilitating multiple interactions in agreement with the spectroscopic data. Our results present complementary insights into the mechanisms of adsorption of TETs on smectites important for their retention in natural and engineered soil environments.

## Introduction

Widely used antibiotics are considered contaminants of emerging concern to human and ecosystem health due to their potential adverse effects on important soil microbial processes (*1*−*6*) and aquatic photosynthetic organisms (*7*−*9*), and their implications in the rise of antibiotic-resistant genes (*10*). Specifically, the tetracycline (TET) antibiotics, commonly used in both human and veterinary medicine, have been shown to disrupt microbial soil respiration (*1, 3*), Fe(III) reduction (*4*), nitrification (*2*), and phosphatase activities (*3*) but these effects can be mitigated when these antibiotics are adsorbed in the soil matrix (*1, 11, 12*). For instance, antibiotics adsorbed to montmorillonite-rich soils exhibit very low desorption and minimal antibacterial activity but there was significant growth inhibition of soil bacteria incubated with antibiotics bound to kaolinitic soils (*11, 12*). These findings implied that bioavailability of antibiotics may be impeded by their physical exclusion in the interlayers of smectite-type clay minerals (2:1 phyllosilicates), including montmorillonite (MONT), prevailing in temperate-zone soils. Of specific interest are the mechanisms of retention by smectites as a prerequisite to assessing the implication of these clay minerals in the fate of antibiotics in natural soils and their potential application in waste treatment and containment.

The formation of TET−MONT complexes has been the subject of several investigations. Adsorption studies (*13*−*19*) and X-ray diffraction (XRD) analyses (*16*−*19*) have revealed high adsorption and intercalation of TETs in the MONT interlayer space at acidic pH, whereas, at circumneutral to basic pH, /low adsorption suggests weak surface complexation and intercalation was significant only in the presence of divalent cations. These results imply that the interlayer adsorption of TETs is pH-dependent according to favorable speciation of the adsorptive and the adsorbent to mediate electrostatic interactions between the negatively charged MONT surface and the positively charged TET species. Nonionic interactions were also suspected (*16*). Infrared (IR) spectroscopic analyses of TET−smectite complexes (*16*−*19*), thus far the only direct experimental elucidation of the above interactions, indicate that the TET moieties may be involved in hydrogen bonding and $\pi-\pi$ interactions, in addition to cationic exchange and cation complexation, but nuclear magnetic resonance (NMR) spectroscopy was suggested (*17*) in order to resolve these interactions as a function of pH. Moreover, a "tilted" orientation of TET antibiotics in the MONT interlayer space was inferred from X-ray data (*16, 17*) and a recent computational study (*20*) of electrostatic potential maps of TETs and other antibiotics further stresses that specific antibiotic structures may be important for favorable interactions with different minerals. Therefore, an investigation that provides improved molecular characterization of TET−MONT complexes and considers the constraints of the antibiotic and mineral structures seems warranted.

The aim of the present study is to integrate complementary spectroscopic analyses, XRD, IR, $^{1}H-^{13}C$ NMR, $^{23}Na$ NMR, and computational simulations in an effort to provide a comprehensive elucidation of the complexation mechanisms of oxytetracycline (OTC; see Figure 1A and B for structure and speciation), a commonly used TET antibiotic, by Na-saturated MONT (Na-MONT) at different pH values. A Fe-free synthetic MONT (*21*) was used to minimize interference, during the spectroscopic analyses, from paramagnetic constituents (e.g., Fe) typically present in natural clay structures. We resolved the speciation of adsorbed OTC and identified the functional groups mediating the OTC-MONT complex using, in concert, the $^{1}H-^{13}C$ NMR signature of OTC and the IR bending and stretching vibration bands of OTC moieties. In addition to XRD, the NMR profile of the $^{23}Na$ nuclei was recorded to probe the different sites of OTC adsorption on the clay mineral surface. We then explored the favorable binding conformations of the intercalated OTC and assessed the interactions deduced from the spectroscopic experiments

* Corresponding author phone: (609) 258-9097; fax: (609) 258-3565; e-mail: ludmilla@princeton.edu.
† Environmental Geochemistry Group.
‡ Equipe Matériaux à Porosité Contrôlée.
§ Mineralogy and Environments Group.
∥ Institut Universitaire de France.
⊥ Present address: Institute of Integrative Genomics, Carl Icahn Laboratory, Princeton University, Princeton, NJ 08540.

10.1021/es102136y 
Published on Web 09/24/2010

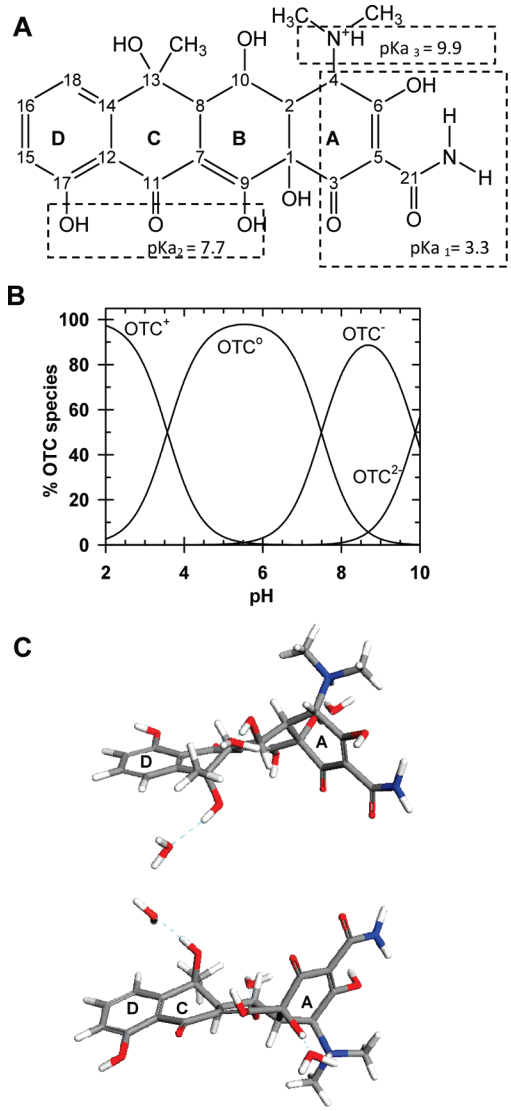


**FIGURE 1. Structure (A) and ionization scheme (B) of OTC. In (A), ionizable functional groups and corresponding p$K_a$ values are shown. (C) Two views of a molecular dynamics-optimized hydrated fully protonated OTC (noncoordinated waters were removed for clarity). Color legend for the atoms in (C): C (gray), O (red), N (blue), and H (white).**

by performing Monte Carlo molecular simulations of OTC adsorption in a model MONT interlayer space.

## Materials and Methods

**Materials.** Oxytetracycline-hydrochloride (>99% purity) and all other chemicals (analytical grade) were obtained from Sigma-Aldrich. The Fe-free synthetic Na-MONT [$Na_{0.30}(Si_4)$-$(Al_{1.70}Mg_{0.30})O_{10}(OH)_2$], which was synthesized as described previously (*21*), has an XRD pattern similar to Wyoming Na-MONT (*22*).

**Adsorption Experiments.** The adsorption experiments were performed by adding 20.0 mL of 320 $\mu$M OTC to 0.02 g (dry weight) of MONT in PTFE tubes, wrapped in two layers of aluminum foil to avoid OTC photodegradation. The OTC solutions were prepared with deionized water (Milli-Q gradient system—resistivity >18 MΩ cm) in 0.01 M $NaNO_3$ with 5 mM each of an acetate/bicarbonate ($NaCH_3COO$/$NaHCO_3$) buffer, brought to pH 4.0, 5.0, 6.0, or 8.0 by additions of $HNO_3$ aliquots. The final pH after the adsorption experiment was systematically within 0.1 pH unit of the initial pH. The adsorption experiments were conducted at room temperature for 40 h; kinetic experiments showed no significant changes in OTC adsorption after 12 h. The OTC-clay suspension was centrifuged at 2500*g* for 20 min and, after filtering the supernatant through a 0.22 $\mu$m polycarbonate filter (Fisher), the concentration of OTC was determined by UV−vis analysis using a Perkin-Elmer Lamda35 spectrophotometer. The absorbance of the OTC was measured at 356 nm at pH 4, pH 5, and pH 6, and at 360 nm at pH 8 (*23*). Less than 5% of the OTC was determined to be lost by adsorption to the tube and the filter from blank experiments.

**X-ray Diffraction Analysis.** Oriented slides were prepared by carefully pipetting the OTC-clay suspension, following the 40-hr adsorption reaction under the different pH conditions, onto a glass slide. The samples were equilibrated then measured at constant temperature (25 °C) and constant relative humidity (20%). The XRD patterns were recorded with a Bruker D5000 diffractometer operated at 40 kV and 40 mA and equipped with an Ansyco rh-plus 2250 humidity control device coupled to an Anton Paar TTK450 chamber. The scanning parameters were 0.02° 2$\theta$ step size and 8 s as counting time per step over 1−10° ($\lambda$ = 1.5418 Å).

**Solid-State NMR and FTIR Measurements.** The OTC-MONT samples for these measurements were prepared as described for the adsorption experiments at pH 4 and pH 8. In preparation for spectroscopic measurements, the samples were freeze-dried following the centrifugation step (*17*). Solid state NMR spectra were recorded using a Bruker Avance II 400WB instrument on samples packed in a 4-mm diameter cylindrical zirconia rotor. The $^{23}$Na magic angle spinning (MAS) NMR spectra were recorded with a $\pi/8$ pulse duration of 0.75 $\mu$s, 1 s recycle delay and a spinning frequency of 12 kHz, the $^{23}$Na chemical shifts being relative to 1 M NaCl solution. The $^1$H−$^{13}$C cross-polarization MAS (CPMAS) NMR spectra were recorded with the spectrometer operating at $B_0$ = 9.4T and 100.2 MHz. Samples were spun at 10 kHz. The $^1$H−$^{13}$C CPMAS NMR measurements were performed with a proton $\pi/2$-pulse duration of 3.2 $\mu$s, a contact time of 1 ms, and a recycle delay of 4 s. The dipolar dephasing $^1$H−$^{13}$C CPMAS NMR spectra were recorded with a rotor synchronized dephasing delay of 40 $\mu$s between cross-polarization and decoupling as previously suggested (*24*) for organic solids; the $^1$H and $^{13}$C chemical shifts are relative to tetramethylsilane.

Using a Bruker Equinox 55 spectrometer with a DTGS detector, FTIR measurements were performed both on the freeze-dried OTC-MONT samples and on the same samples subjected to further dehydration for 12 h at temperatures not exceeding 100 °C in order to minimize typical thermal degradation of OTC (*25*). The number of scans was 100 and the resolution 2 $cm^{-1}$. Pellets of the materials were prepared using IR-grade potassium bromide (Fisher).

**Molecular Simulation of OTC Intercalation.** An exploratory study of the binding conformations of cationic OTC in the MONT interlayer space was conducted. The simulated cell of the model MONT [$Na_{0.75}(Si_{7.75}Al_{0.25})(Al_{3.5}Mg_{0.5})O_{20}(OH)_4$] contains a total charge of −6 resulting from isomorphic substitutions: two in the tetrahedral sites (Si → Al) and four in the octahedral sites (Al → Mg) (*29*). Geometry-optimized hydrated OTC (Figure 1C) was obtained, following the computational method of Aristilde and Sposito (*26*), by subjecting a nonperiodic simulation cell of OTC within a 2.00 × 2.00 × 2.00 $nm^3$ box of explicit water molecules through both energy minimization and molecular dynamics algorithms using the condensed-phase optimized molecular potentials for atomistic simulation studies (COMPASS) force-field (*27*) with the Discover module of the Materials Studio software package (*28*). Different possible configurations of OTC were tested during the optimization procedure and the lowest-energy configuration was used. The COMPASS force-field, previously employed in the simulation of the hydrated model MONT interlayer space (*29*), was validated here for

appropriate description of the hydrated OTC by providing bond angles and bond lengths in agreement with structural data (*30*) (Supporting Information (SI), Appendix A). Moreover, the conformation of the optimized OTC molecule (Figure 1C) is characteristic of related TET molecules wherein the rings A and B are in a half-chair conformation, the ring C in a boat conformation, and the D ring in a planar configuration (*30, 31*).

Following validation, the COMPASS force-field was used with the Adsorption Locator module of Materials Studio (*28*) to simulate the adsorption of the optimized cationic OTC in the model MONT interlayer space within a periodic cell, 2.11 nm ×1.83 nm × basal spacing ($d_{001}$). An annealing Monte Carlo search of the lowest-energy OTC-MONT system was performed by subjecting the adsorptive molecules, 5 $Na^+$ and 1 hydrated cationic OTC (i.e., OTC with its three solvated $H_2O$, Figure 1C), through both translation and rotation steps with respect to the surface of the MONT layers during a temperature cycle from 300 to 800 K, repeated three times. This annealing procedure allows testing of different conformations in the intercalation of the adsorptive molecules, which was monitored with $d_{001}$ from 1.25 nm, typical for monohydrated Na-MONT (*32*), to 1.40 nm, 1.50 nm, 1.60 nm, 1.80 nm, and 1.90 nm. At each $d_{001}$, the MONT interlayer was optimized first with 6 $Na^+$ in the interlayer and, after removing one $Na^+$, it was simulated with the mixed occupancy. To examine the influence of the localization of the clay structural charge on the conformation of OTC in the interlayer space, we simulated two scenarios at each $d_{001}$ wherein the $Na^+$ removed was compensating an isomorphic substitution site from either the octahedral sheet or from the tetrahedral sheet.

## Results and Discussion

**Adsorption and Intercalation of OTC.** Similar to previous reports (*13*−*15*), the amount of OTC adsorbed on MONT significantly decreases as pH increases: 256.3 ± 17.9, 157.9 ± 18.8, 111.4 ± 9.6, and 84.4 ± 11.2 × $10^3$ $\mu$mol OTC/g MONT at, respectively, pH 4, 5, 6, and 8 (Figure 2A). In the absence of OTC, $d_{001}$ of MONT, calculated from the 001 reflection, ranges from 1.25 to 1.28 nm. Following the adsorption of OTC on MONT, $d_{001}$ was 1.83, 1.76, 1.35, and 1.28 nm at, respectively, pH 4, 5, 6, and 8 (Figure 2B). Intercalation of the buffer components was not observed (data not shown). Therefore, changes in the 001 reflection are due to OTC entry in the MONT interlayer space. Our XRD results thus indicate significant OTC intercalation at pH 4 and pH 5, relatively less at pH 6, and no intercalation at pH 8 under our experimental conditions (Figure 2B). Therefore, at circumneutral and alkaline pH, OTC adsorption may be primarily on the MONT external sites, compensating for negative charges arising either from structurally charged or deprotonated sites on the basal and edge surfaces (*33*). The positive correlation between the intercalation of OTC in the MONT interlayers and the amount of OTC adsorbed on MONT as a function of pH suggests that increase in the ionization of both OTC species and MONT may play a role in impeding the interlayer adsorption of OTC.

**$^1$H−$^{13}$C MAS NMR.** These NMR experiments were first conducted in the absence of MONT in order to assign specific chemical shifts to the C atoms of OTC (Figure 3A). Due to the multiple line widths and intensities, (Figure 3B), a dipolar dephasing NMR experiment (*24*) was also performed and the resulting assignment of the resonances was consistent with previous chemical assignments of OTC (*34*) (SI, Appendix C). Following the adsorption of OTC with MONT, it was possible to identify at least 15 resonances of the $^1$H−$^{13}$C CPMAS NMR spectra of the antibiotic (Figure 3B) wherein significant changes in the resonance signature were probed to obtain information on the adsorbed OTC.

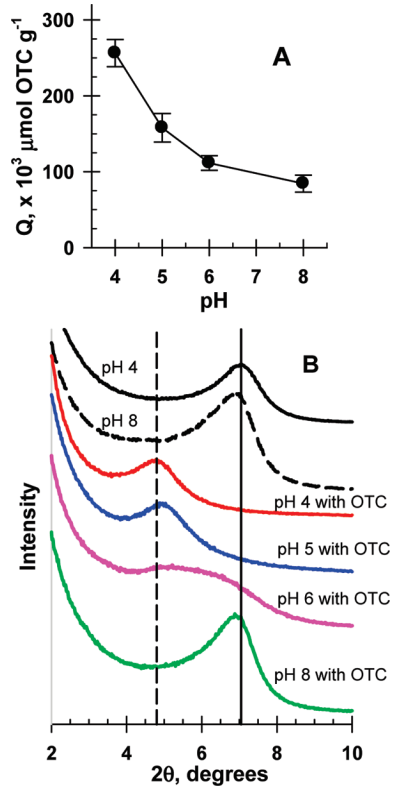


**FIGURE 2. (A) Adsorbed amount of OTC on MONT (Q) as a function of pH and (B) X-ray diffraction patterns of MONT in the absence of OTC at pH 4 (black line) and pH 8 (black dashes) and in the presence of adsorbed OTC at pH 4 (red), pH 5 (blue), pH 6 (pink), and pH 8 (green). In (A), the symbols and the error bars represent, respectively, averaged and standard deviation values from three replicates. In (B), the solid and dotted lines represent, respectively, $d_{001}$ of 1.25 and 1.84 nm.**

Significant changes in the chemical shifts of $C_3$, $C_5$, $C_9$, and $C_{11}$ resonances reflect the presence of different species of OTC (*34*). The disappearance of the $C_5$ resonance (Figures 3A and 3B) is likely a consequence of the ionization of the hydroxyl group on $C_6$ of OTC with p$K_a$ of 3.3 (Figure 1A), which induces charge delocalization across $C_6$, $C_5$, and $C_3$ (*34*). Changes in the other C resonances provide insight into which C atom, $C_9$ or $C_{17}$, is associated with the deprotonated OH of the second ionizable group of OTC (Figure 1A). The appreciable decrease in the relative line intensities for both $C_3$ and $C_{11}$ (Figure 3B) at pH 8 suggests the deprotonation of the OH group associated to $C_9$ and the lack of significant changes in the chemical shifts of the aromatic C atoms vicinal to $C_{17}$ (i.e., $C_{12}$, $C_{14}$−$C_{16}$, and $C_{18}$) confirms that the OH group at $C_{17}$ was not deprotonated as predicted previously from theoretical molecular orbital calculations (*35*). In sum, we deduce that the adsorbed OTC species are in accordance with the ionization scheme of OTC: zwitterionic species at pH 4 and anionic species at pH 8 (Figure 1B).

The appreciable broadening (relative to OTC alone) of the resonances indicates a restricted mobility of OTC at both pH 4 and pH 8 in the presence of MONT (Figure 3B) as a result of the interactions of the adsorbed OTC species, which are in the MONT interlayer space at pH 4 and predominantly on the external sites at pH 8 according to XRD. The identity of these interactions was investigated by FTIR, $^{23}$Na NMR, followed by molecular simulations.

**FTIR Analysis.** Spectra recorded on OTC alone and MONT alone were used as references (Figure 3C). The most characteristic bands of OTC are in the 1100−1750 cm$^{-1}$ region (SI, appendix D). As previously pointed out (*17*), the absence of significant IR peaks from Na-MONT in this region is

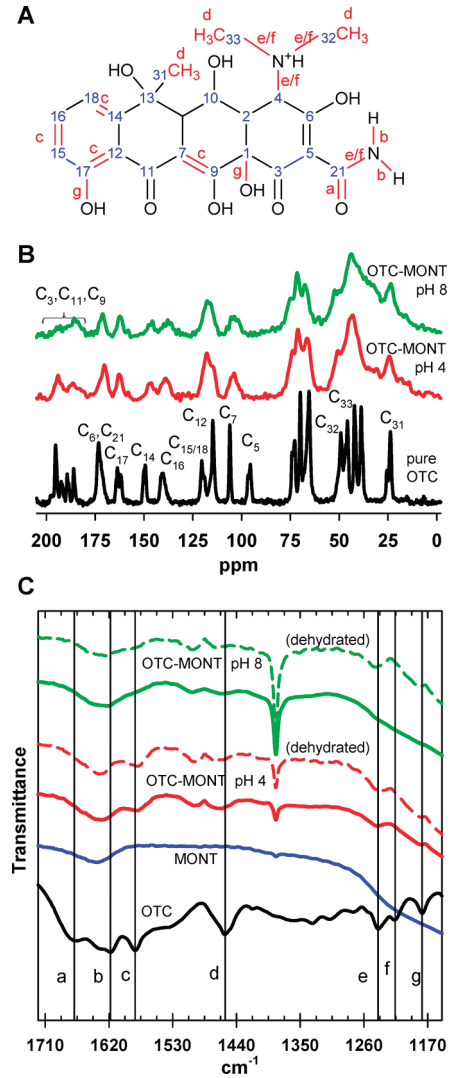


**FIGURE 3. Structure of OTC (A), and $^{1}H-^{13}C$ CPMAS NMR (B) and FTIR (C) spectra of OTC in the absence and presence of MONT. The OTC structure shows the assigned IR vibration bands (a–g) and the numbers assigned to the C atoms for the NMR analysis (See the Results and Discussion for details). The dashed lines in (C) represent spectra obtained with samples subjected to further dehydration (see the Materials and Methods section). Color legend: MONT alone (blue), fully protonated OTC alone (black), OTC-MONT at pH 4 (red), OTC-MONT at pH 8 (green).**

important for identifying the OTC interaction with MONT. Changes in the following vibration bands were monitored: the antisymmetric $CH_3$ deformation band at 1456 $cm^{-1}$ (d), the double amino C—N stretching bands at 1240 and 1216 $cm^{-1}$ (e and f), the C═O (or amide I) stretching and the —N—H (or amide II) bending bands of the amide moiety at, respectively, 1669 $cm^{-1}$ (a) and 1618 $cm^{-1}$ (b), the aromatic C═C stretching band at 1583 $cm^{-1}$ (c), and the phenolic C—O stretching band at 1178 $cm^{-1}$ (g) (Figure 3C) (*36*). At pH 4, the IR spectrum of the freeze-dried sample was the same as that of the sample dehydrated whereas, at pH 8, the two IR spectra were different, this difference being used to identify moieties possibly interacting with water molecules (Figure 3B).

The major decrease of the $CH_3$ vibration band at 1456 $cm^{-1}$ (d) and the appearance of a doublet of $CH_3$ vibration bands at 1506 and 1475 $cm^{-1}$, at both pH 4 and pH 8, indicate an interaction involving the protonated dimethylamino group, in accordance with the lower mobility of the $CH_3$ moieties observed by $^{1}H-^{13}C$ CPMAS. We note that there are four possible C—N bonds (Figure 3): one associated with the amide group and three with the dimethylamino group. The disappearance of the C—N stretching band at 1216 $cm^{-1}$ (f) may therefore be a consequence of the proposed involvement of the latter group in the mechanisms of OTC interaction with MONT. The C—N stretching band at 1240 $cm^{-1}$ (e) appears unchanged after OTC adsorption at pH 4 and, after further dehydration, also at pH 8 and was therefore presumed to be associated with the amide moiety. The amide moiety is likely interacting with water molecules at pH 8.

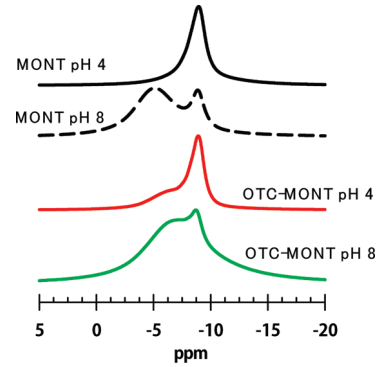


**FIGURE 4. $^{23}Na$ solid-state NMR of MONT in the absence of OTC at pH 4 (black solid line) and pH 8 (black dashed line) and in the presence of adsorbed OTC at pH 4 (red solid line), and pH 8 (green solid line).**

The significant suppression of the C═O amide I stretching band (Figure 3C, a) was suggested previously (*17*) to result from the complexation of MONT-associated metals by the amide O. By contrast, the —N—H amide II bending band (Figure 3C, b) is minimally affected, suggesting little involvement of the amide $NH_2$ moiety in the OTC interaction with the MONT, which is consistent with the proposed participation of this group in stabilizing a TET conformation by mediating intramolecular H-bonding interaction with the vicinal carbonyl O group (*34*) (Figure 1C).

The aromatic C═C stretching band at 1583 $cm^{-1}$ (Figure 3C, c) was detected for OTC-MONT at pH 4 but was no longer distinguishable for OTC-MONT at pH 8. Aromatic C═C bonds are associated with the two OH groups that can undergo deprotonation around pH 8 (Figure 1A) and, therefore, their stretching vibration bands may be affected by the deprotonation of the phenolic OH group attached to $C_{17}$ or the OH group linked to $C_9$. As the phenolic C—O stretching band (Figure 3C, g) at 1178 $cm^{-1}$ is detected at pH 4 and, after further dehydration, at pH 8, we propose that the deprotonation occurs on the OH bonded to $C_9$, which is consistent with the $^{13}C$ NMR results and theoretical calculations (*35*) as previously discussed. At pH 8, this latter vibration band appears only after further dehydration, suggesting interactions between water molecules and phenolic OH groups of OTC.

**$^{23}Na$ NMR.** In the absence of OTC, the isotropic region of the $^{23}Na$ NMR spectra reveals two distinct resonances: a sharp one at −8.9 ppm detected at both pH 4 and pH 8 and a broad one at −5.2 ppm peak detected only at pH 8 (Figure 4). The sharp peak is indicative of a symmetric environment of Na cations surrounded by its solvated hydration shell, which corresponds to hydrated interlayer Na cations in the MONT interlayer space (*37*). By contrast, the breadth of the downfield peak at pH 8 corresponds to Na atoms in a distribution of environments. The characteristic of this peak likely reflects Na cations involved in inner-sphere complexation with edge sites (*33*).

In the presence of OTC, the two environments of Na cations were altered (Figures 4). At pH 4, the appearance of a shoulder downfield of the sharp peak indicates a

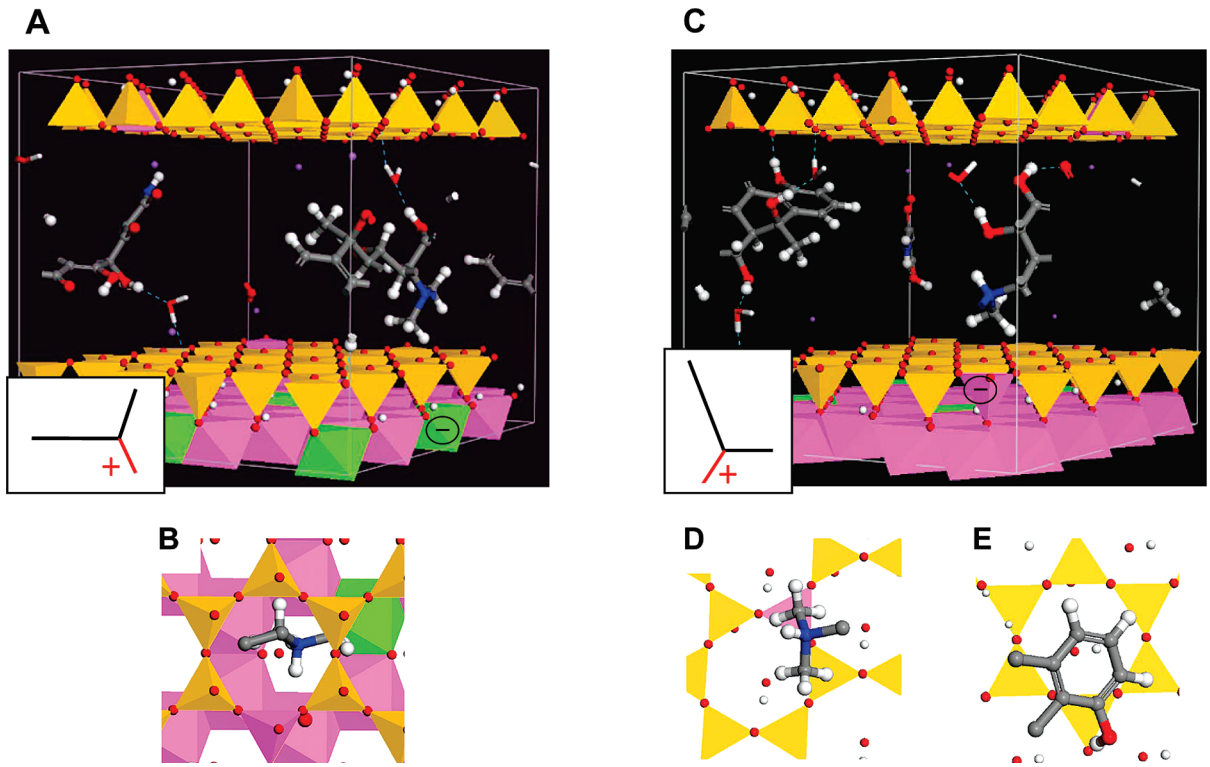


**FIGURE 5. Views of the optimized adsorptive structure of hydrated cationic OTC compensating a negative charge localized in the octahedral sheet (A and B) or in the tetrahedral sheet (C, D, E) of the Na-MONT with $d_{001}$ = 1.8 nm. In (A) and (C), the OTC conformation in one unit cell is shown—see Appendix E in SI for extended multiple-cell views; dotted lines represent H-bonds and the inserts show a schematic of the OTC orientation in the interlayer space. In (B) and (D), a close-up view from above of the OTC dimethyl amino group is shown and, in (E), a close-up view from below of the OTC fully conjugated aromatic ring is shown (some OTC atoms in (B), (D), and (E), and the octahedral sheet in (E) are removed for clarity). Both OTC and water molecules are shown in a ball-and-stick motif, the Na ions are represented by small spheres, and the clay structure is shown in a polyhedron-and-ball motif. Color code: gray, (C), red (O), white (H), blue (nitrogen), yellow (Si), pink (Al), green (Mg), and purple (Na).**

modification of the Na environment, which may reflect the disturbed environment of the interlayer Na cation in the presence of intercalated OTC, as shown by XRD. The complexation of Na cations by deprotonated OTC phenol groups in the interlayer space, as suggested by the IR spectra, may be responsible for this new $^{23}$Na NMR environment. The simultaneous presence of undisturbed environment of interlayer Na cations at pH 4 (Figure 4) as represented by the sharp peak, is likely a consequence of segregation of OTC in specific interlayers, in accordance with the amount of adsorbed OTC (256.3 ± 17.9 mmol/kg clay), which is insufficient to compensate fully for the MONT permanent charge [440 $mmol_c$/kg (*22*)]. At pH 8, the $^{23}$Na signal is significantly broadened indicating the existence of possible multiple Na environments and the sharp peak observed in the absence of OTC is still present (Figure 4). This presence of interlayer Na cations is consistent with the lack of appreciable intercalation of OTC at pH 8, as determined by XRD (Figure 2B). However, the relative height and broadness of the signals indicate that, in comparison to pH 4, Na environments other than those in the MONT interlayer space may be predominant at pH 8, perhaps due to the multiple Na complexation sites including the ionizable sites of adsorbed OTC. Indeed, the upfield shift of the broad peak from −5 ppm to −6.5 ppm, respectively in the absence and presence of OTC at pH 8, indicates the presence of Na environment distinct from that of Na cations associated with the MONT edge sites in the absence of OTC.

**Binding Mechanisms and Structures.** To the best of our knowledge, this study presents the first attempt to elucidate the interactions of a tetracycline antibiotic with MONT using many direct molecular methods. As in previous studies (*17, 19*), our XRD patterns indicate a decrease in the interlayer adsorption of OTC as a function of increasing pH, which has led to the proposal that OTC is adsorbed primarily on the external basal and edge surfaces of monovalent-saturated MONT under circumneutral and alkaline pH conditions. To corroborate these sites of OTC adsorption, we were able to capture the disturbed molecular environment of the MONT-associated Na cations and possible Na complexes with OTC. At both pH 4 and pH 8, in the IR deformation and stretching vibration bands associated with the dimethylamino group of OTC are consistent with a binding mechanism involving this group, which was proposed to mediate electrostatic interactions of the antibiotic with the negatively charged surface sites of the clay (*17*). Due to similarities in the $^{1}$H−$^{13}$C CPMAS NMR spectra of OTC in the presence of MONT at both pH, we suggest a similar binding conformation of adsorbed OTC in the interlayer space and on the external basal surface of the clay.

To determine the binding structures of the intercalated OTC facilitating the interactions deduced from the spectroscopic analyses, we performed molecular simulations of an optimized hydrated cationic OTC with a model MONT interlayer space. The conformation of the optimized OTC is similar to the one proposed for tetracycline under both acidic and neutral pH conditions (*19, 30, 31*), thus allowing our computational results to provide molecular insight into the intercalation of a range of TET species. The Monte Carlo-simulated interlayer adsorption reveals the most thermodynamically favorable adsorbate structures within a MONT basal spacing of 1.8 nm, which is in agreement with 001 reflection of OTC-MONT at pH 4 (Figure 2B), according to the XRD data previously discussed. We observed that the OTC positive charge was superimposed

on the cavity adjacent to the negative charge from the octahedral sheet (Figure 5A and B) but directly on the negative charge from the tetrahedral sheet (Figure 5C and D). This difference in OTC binding, which may be a consequence of the greater delocalization of the negative charges on the O atoms of the octahedron than those of the tetrahedron (*38*), leads to different orientations of the OTC molecule in the interlayer space. Similar to the optimal positioning previously proposed (*20*) for the intercalated OTC in MONT, the OTC orientation with the charged octahedral sheet is parallel to the basal surface. This orientation may be the most relevant to our experiments whereby the permanent charge of the MONT clay arises from charges in the octahedral sheet. On the other hand, the interaction of the OTC with the charged tetrahedral sheet facilitates a different OTC orientation with the fully conjugated aromatic ring toward the MONT siloxane cavity (Figure 5E), perhaps to assist in the anchorage of OTC in the interlayer space by mediating a $\pi$-siloxane ring interaction (*39*).

Hydrogen bonding interactions were proposed in TET−MONT complexes (*13, 16, 17*). The simulated intercalated OTC conformations reveal one H-bond interaction between an OH group of OTC and a basal O atom and two additional water-bridged interactions between OH groups of OTC and two O atoms of the mineral surface (Figure 5A and C). These latter interactions were also inferred from the IR data at pH 8. We also note that the OTC amide carbonyl O coordinates a Na cation, in accordance with the changes in both the IR stretching vibration band of amide I and the $^{23}$Na NMR environments.

The present study employs the combination of modeling and experimental techniques to provide new insights into how smectite-type clay minerals may act as an effective scavenger in natural and engineered sequestration of antibiotics and other polar organic contaminants. In sum, the spectroscopic results corroborate cation-exchange, cation complexation, and H-bonding interactions in TET−smectite complexes and the molecular modeling results demonstrate that specific interlayer space expansion and structural charge localization may predict favorable binding conformations to facilitate these interactions. Our modeling results further imply that, in addition to favorable chemical speciation, the structural characteristics of the soil mineral composition may control the adsorption behavior and retention of tetracycline antibiotics in the soil environment.

## Acknowledgments

We are grateful to Audrey Perrier, Florian Molton, Martine Lanson, and Delphine Tisserand of University of Grenoble and Mark Johnson of the Institut Max Laue-Langevin for technical assistance, to Rebecca Sutton of the Environmental Working Group for providing the model clay, and to Sara S. Rocks of Princeton University for helpful discussion on the NMR analysis. This work was supported by a grant from the Centre Nationale de Recherche (CNRS).

## Supporting Information Available

Bond lengths and bond angles in molecular dynamics-optimized OTC; $^{1}$H−$^{13}$C CPMAS NMR of oxytetracycline with and without dipolar dephasing; infrared spectra assignments for OTC; extended views of simulated OTC conformation in the MONT interlayers. This material is available free of charge via the Internet at http://pubs.acs.org.

## Literature Cited

(1) Zielezny, Y.; Groeneweg, J.; Vereecken, H.; Tappe, W. Impact of sulfadiazine and chlorotetracycline on soil bacterial community structure and respiratory activity. *Soil Biol. Biochem.* **2006**, *38*, 2372–2380.

(2) Halling-Sørensen, B. Inhibition of aerobic growth and nitrification of bacteria in sewage sludge by antibacterial agents. *Arch. Environ. Contam. Toxicol.* **2001**, *40*, 451–460.

(3) Boleas, S.; Alonso, C.; Pro, J.; Fernández, C.; Carbonell, G.; Tarazona, J. V. Toxicity of the antimicrobial oxytetracycline to soil organisms in a multi-species-soil system (MS center dot 3) and influence of manure co-addition. *J. Hazard. Mater.* **2005**, *122*, 233–241.

(4) Thiele-Bruhn, S.; Beck, I.-C. Effects of sulfonamide and tetracycline antibiotics on soil microbial activity and microbial biomass. *Chemosphere* **2005**, *59*, 457–465.

(5) Córdova-Kreylos, A. L.; Scow, K. M. Effects of ciprofloxacin on salt marsh sediment on microbial communities. *ISME J.* **2007**, *1*, 585–595.

(6) Boleas, S.; Alonso, C.; Pro, J.; Babín, M. M.; Fernández, C.; Carbonell, G.; Tarazona, J. V. Effects of sulfachlorpyridazine in MS.3-arable land: A multispecies soil system for assessing the environmental fate and effects of veterinary medicines. *Environ. Toxicol. Chem.* **2005**, *24*, 811–819.

(7) Richards, S. M.; Wilson, C. J.; Johnson, D. J.; Castle, D. M.; Lam, M.; Mabury, S. A.; Sibley, P. K.; Solomon, K. R. Effects of pharmaceutical mixtures in aquatic microcosms. *Environ. Toxicol. Chem.* **2004**, *23*, 1035–1042.

(8) Wilson, C. J.; Brain, R. A.; Sanderson, H.; Johnson, D. J.; Bestari, K. T.; Sibley, P. K.; Solomon, K. R. Structural and functional responses of plankton to a mixtrue of four tetracyclines in aquatic microcosms. *Environ. Sci. Technol.* **2004**, *38*, 6430–6439.

(9) Aristilde, L.; Melis, A.; Sposito, G. Inhibition of photosynthesis by a fluoroquinolone antibiotic. *Environ. Sci. Technol.* **2010**, *44*, 1444–1450.

(10) Knapp, C. W.; Dolfing, J.; Ehlert, P. A. I.; Graham, D. W. Evidence of increasing antibiotic resistance gene abundances in archived soils since 1940. *Environ. Sci. Technol.* **2010**, *44*, 580–587.

(11) Soulides, D. A.; Pinck, L. A.; Allison, F. E. Antibiotics in soils: V. Stability and release of soil-adsorbed antibiotics. *Soil. Sci.* **1962**, *94*, 239–244.

(12) Chander, Y.; Kumar, K.; Goyal, S. M.; Gupta, S. C. Antibacterial activity of soil-bound antibiotics. *J. Environ. Qual.* **2005**, *34*, 1952–1957.

(13) Sithole, B. B.; Guy, R. D. Models for tetracycline in aquatic environments. *Water, Air, and Soil Poll.* **1987**, *32*, 315–321.

(14) Figueroa, R. A.; Leonard, A.; Mackay, A. A. Modeling tetracycline antibiotic sorption to clays. *Environ. Sci. Technol.* **2004**, *38*, 476–483.

(15) Wang, Y. J.; Jia, D.-A.; Sun, R.-J.; Zhu, H.-W.; Zhou;Zhou, D.-M. Adsorption and cosorption of tetracycline and Copper(II) on Montmorillonite as affected by solution pH. *Environ. Sci. Technol.* **2008**, *42*, 3254–3259.

(16) Porubcan, L. S.; Serna, C. J.; White, J. L.; Hern, S. L. Mechanism of adsorption of clindamycin and tetracycline by montmorillonite. *J. Pharm. Sci.* **1978**, *67*, 1081–1087.

(17) Kulshrestha, P.; Giese, R. F., Jr.; Aga, D. S. Investigating the molecular interactions of oxyteracycline in clay and organic matter: Insights on factors affecting its mobility in soil. *Environ. Sci. Technol.* **2004**, *38*, 4097–4105.

(18) Parolo, M. E.; Savini, M. C.; Vallés, J. M.; Baschini, M. T.; Avena, M. J. Tetracycline adsorption on montmorillonite: pH and ionic strength effects. *J. Appl. Clay Sci.* **2008**, *40*, 179–186.

(19) Chang, P.-H.; Jean, J.-S.; Jiang, W.-T.; Li, Z. Mechanisms of tetracycline on rectorite. *Colloid Surf., A* **2009**, *339*, 94–99.

(20) Carasquillo, A. J.; Bruland, G. L.; MacKay, A. A.; Vasudevan, D. Sorption of ciprofloxacin and oxytetracycline zwitterions to soils and soil minerals: influence of compound structure. *Environ. Sci. Technol.* **2008**, *42*, 7634–7642.

(21) Reinholdt, M.; Miéhé-Brendlé, J.; Delmotte, L.; Le Dred, R.; Tuilier, M.-H. Synthesis and characterization of montmorillonite-type phyllosilicates in a fluoride medium. *Clay Min.* **2005**, *40*, 177–190.

(22) Géhin, A.; Grenèche, J.-M.; Tournassat, C.; Brendlé, J.; Rancourt, D. G.; Charlet, L. Reversible surface-sorption-induced electron-transfer oxidation of Fe(II) at reactive sites on a synthetic clay mineral. *Geochim. Cosmochim. Acta* **2007**, *71*, 863–876.

(23) Schmitt, M. O.; Schneider, S. Spectroscopic investigation of complexation between various tetracyclines and $Mg^{2+}$ or $Ca^{2+}$. *Phys. Chem. Comm.* **2000**, *3*, 42–55.

(24) Witt, J.; Fenzke, D.; Hoffmann, W.-D. Investigation of the dipolar dephasing NMR on organic solids. *Appl. Magn. Reson.* **1992**, *3*, 151–163.

(25) Hassani, M.; Lázaro, R.; Pérez, C.; Condón, S.; Pagán, R. Thermostability of oxytetracycline, tetracycline, and doxycycline at ultrahigh temperatures. *J. Agric. Food Chem.* **2008**, *56*, 2676–2680.

(26) Aristilde, L.; Sposito, G. Molecular modeling of metal complexation by a fluoroquinolone antibiotic. *Environ. Toxicol. Chem.* **2008**, *27*, 2304–2310.
(27) Sun, H. COMPASS: An ab initio force-field optimized for condensed-phase applications-overview with details on alkane and benzene compounds. *J. Phys. Chem. B* **1998**, *102*, 7338–7364.
(28) *Materials Studio*, version 4.2; Accelrys Corporation: San Diego, CA, 2001.
(29) Sutton, S.; Sposito, G. Molecular simulation of humic substance-Ca-montmorillonite complexes. *Geochim. Cosmochim. Acta* **2006**, *70*, 3566–3581.
(30) Koziol, A. E.; Davis, J.; Palenik, R. C.; Palenik, G. J. Structural studies of two tetracyclines: 4-dedimethylaminotetracycline hydrate and 6-methylene-5-oxytetracycline hydrochloride. *J. Crystallogr. Spectrosc. Res.* **1992**, *22*, 493–501.
(31) Othersen, O. G.; Waibel, R.; Lanig, H.; Gmeiner, P.; Clark, T. SCRF-DFT and NMR comparison of tetracycline and 5a,6-anhydrotetracycline in solution. *J. Phys. Chem. B.* **2006**, *110*, 24766–24774.
(32) Ferrage, E.; Lanson, B.; Sakharov, B. A.; Drits, V. A. Investigation of smectite hydration properties by modeling experimental X-ray diffraction patterns: Part I. Montmorillonite hydration properties. *Am. Mineral.* **2005**, *90*, 1358–1374.
(33) Bourg, I. C.; Sposito, G.; Bourg, A. C. M. Modeling the acid-base surface chemistry of montmorillonite. *J. Colloid Interface Sci.* **2007**, *312*, 297–310.
(34) Mooibroek, S.; Wasylishen, R. E. A carbon-13 nuclear magnetic resonance study of solid tetracyclines. *Can. J. Chem.* **1987**, *65*, 357–362.
(35) Othersen, O. G.; Lanig, H.; Clark, T. Systematic surface scan of the most favorable interaction sites of magnesium Ions with tetracycline. *J. Med. Chem.* **2003**, *46*, 5571–5574.
(36) Gunzler, H.; Gremlich, H.-U. *IR Spectroscopy: An Introduction*; Wiley-VCH Verlag GmbH: Weinheim, Germany, 2002.
(37) Ohkubo, T.; Saito, K.; Kanehashi, K.; Ikeda, Y. A study on hydration behaviors of interlayer cations in montmorillonite by solid state NMR. *Sci. Technol. Adv. Mater.* **2004**, *5*, 693–696.
(38) Sposito, G.; Prost, R. Structure of water adsorbed on smectites. *Chem. Rev.* **1982**, *82*, 553–572.
(39) MacKay, A. A.; Seremet, D. E. Probe compounds to quantify cation exchange and complexation interactions of ciprofloxacin with soils. *Environ. Sci. Technol.* **2008**, *42*, 8270–8276.

ES102136Y